

<https://doi.org/10.1038/s42003-025-07686-9>

Strontium isotope mapping of elephant enamel supports an integrated microsampling-modeling workflow to reconstruct herbivore migrations

Check for updates

Deming Yang ^{1,2}✉, Katya Podkovyrovff^{1,3,4}, Kevin T. Uno ^{1,5}, Gabriel J. Bowen ¹, Diego P. Fernandez ¹ & Thure E. Cerling ^{1,3}

Strontium isotope ratios ($^{87}\text{Sr}/^{86}\text{Sr}$) in dental tissues are widely used to study animal and human migration. However, questions remain regarding how different biological processes and sampling methods influence measured $^{87}\text{Sr}/^{86}\text{Sr}$ and subsequent interpretations. We present a unique experiment with the known relocation history of a zoo elephant to evaluate the influence of biological turnover, tissue type, and sampling methods. We collected $^{87}\text{Sr}/^{86}\text{Sr}$ data from the elephant's tusk and molar enamel using in-situ laser ablation microsampling, conventional drilling, and micromilling techniques. Our data comparisons show that the innermost enamel best records the primary $^{87}\text{Sr}/^{86}\text{Sr}$ turnover history, while enamel maturation affects outer enamel $^{87}\text{Sr}/^{86}\text{Sr}$. Conventional drilling and micromilling show attenuated $^{87}\text{Sr}/^{86}\text{Sr}$ records due to enamel maturation and sample averaging. To effectively account for $^{87}\text{Sr}/^{86}\text{Sr}$ signal attenuation due to turnover, we demonstrated a microsampling-modeling workflow using our tusk and enamel data. This recommended workflow can facilitate geospatially explicit interpretations of seasonal migration.

Understanding the biology of extinct species can have profound implications for anthropogenic global change and help us evaluate our impacts on biodiversity¹. Mega-herbivores have played vital roles in both current and past ecosystems with their persistent influences on vegetation dynamics, food web structures, and nutrient cycling². Studies of extinct proboscideans and their behaviors, such as dietary changes, movement/migration, and reproduction, often utilize tracer chemicals and isotopes deposited in mineralized tissues such as tusk dentine and molar enamel^{3–8}. These dental elements can serve as excellent archives of the focal individual because a single tusk or molar may record more than a decade's worth of life history^{9,10}.

Strontium isotopes ($^{87}\text{Sr}/^{86}\text{Sr}$) in mineralized tissues are a powerful tool for reconstructing patterns of movement and migration^{11–16}. This utility is based on the geospatial pattern of $^{87}\text{Sr}/^{86}\text{Sr}$ that depends on the local environment, such as the underlying bedrock geology, soil conditions, dust influxes, and sea spray¹⁷. As animals move across the landscape, they incorporate biologically available $^{87}\text{Sr}/^{86}\text{Sr}$ from the environment (e.g., through food and water) into their incrementally grown tissues (e.g., enamel and dentine), thereby providing histories of their past $^{87}\text{Sr}/^{86}\text{Sr}$ exposures^{18,19}.

High-resolution analytical methods such as laser ablation inductively coupled plasma mass spectrometry (LA-ICP-MS) and geostatistical methods^{20,21} have facilitated tremendous growth in geospatially explicit reconstructions of provenance and movement/migration patterns in extinct proboscideans^{7,22,23}. However, major challenges persist in the efforts to reconstruct movement or migration history from intra-tooth $^{87}\text{Sr}/^{86}\text{Sr}$ data series. One is the lack of longitudinal studies on modern analogs with known movement histories. Another is the lack of systematic comparisons between $^{87}\text{Sr}/^{86}\text{Sr}$ measured in different tissue archives (e.g., enamel and dentine).

Experiments on modern analogs are essential in understanding how isotope tracers record life histories and how they can be applied to extinct taxa^{24,25}. Misha, a female African savanna elephant (*Loxodonta africana*) with a known relocation history (Methods), offers an excellent experimental setting to understand how $^{87}\text{Sr}/^{86}\text{Sr}$ is archived in different dental tissues (Fig. 1). Studies on her enamel and dentine growth, mineralization, and intra-tooth isotopes have facilitated the application of similar tools to extinct species^{26,27}. While tusk dentine is an excellent life history archive, molar enamel is often preferred in archeological and paleontological studies due to

¹Department of Geology and Geophysics, University of Utah, Salt Lake City, UT, 84112, USA. ²Division of Anthropology, American Museum of Natural History, New York, NY, 10024, USA. ³School of Biological Sciences, University of Utah, Salt Lake City, UT, 84112, USA. ⁴Institute of Ecology and Evolution, University of Oregon, Eugene, OR, 97403, USA. ⁵Department of Human Evolutionary Biology, Harvard University, Cambridge, MA, 02138, USA. ✉e-mail: dyang@amnh.org

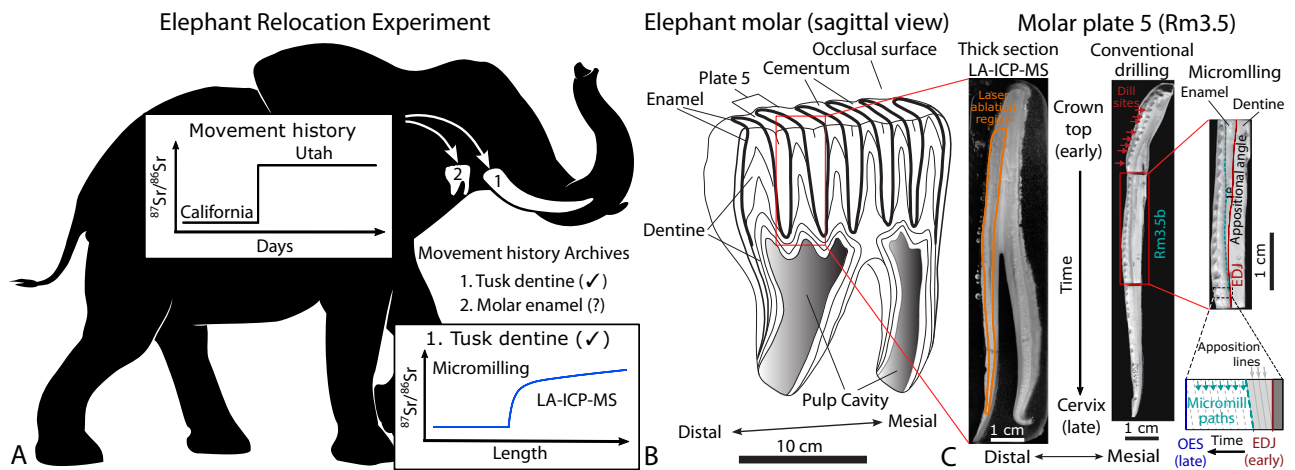


Fig. 1 | Summary of Misha's relocation history, its associated $^{87}\text{Sr}/^{86}\text{Sr}$ archives, and sampling methods used in this study. **A** Schematics of how Misha's $^{87}\text{Sr}/^{86}\text{Sr}$ intake history is recorded in incrementally grown tissues. The tissues include (1) tusk dentine (published)³⁶, and (2) molar enamel (this study). **B** Sagittal section of an elephant molar showing the anatomy of the molar plates, modified from Fisher and Fox¹⁰ with permission. **C** Illustrations of the three sampling methods to recover $^{87}\text{Sr}/^{86}\text{Sr}$ intra-tooth series from the molar plate (Rm3.5): Laser Ablation Inductively Coupled Plasma Mass Spectrometry (LA-ICP-MS),

conventional drilling, and micromilling. Enamel growth starts from the crown top and progresses towards the cervix, and from the enamel-dentine junction (EDJ) towards the outer enamel surface (OES). The orange polygon marks the region of the LA-ICP-MS analysis (details in Methods). The red arrows indicate sites of conventional drilling with grooves on the OES (details in Methods). The turquoise arrows indicate micromilling paths parallel to the enamel apposition lines. Silhouette is modified from the original image by Agnello Picorelli, from <https://www.phylopic.org/>.

its resilience to diagenesis^{28,29}. However, enamel is challenging to work with due to its complex mineralization process. Enamel mineralization comprises a secretion phase whereby less than half of the mineral fraction is deposited onto a protein-rich enamel matrix almost instantaneously, and a maturation phase whereby the remaining mineral fraction is slowly added to the matrix often over the period of months to years^{26,30–32}. As a result, most sampling techniques (e.g., conventional drilling) integrate mineral fractions from the two heterochronous mineralization phases, leading to time-averaging that manifests in the damping of the amplitude and the distortion in the shape of the original isotope variation^{30,32–34}.

For strontium, an overarching question is how enamel archives the longitudinal $^{87}\text{Sr}/^{86}\text{Sr}$ intake/exposure of an individual. We focus on three processes that can influence measured $^{87}\text{Sr}/^{86}\text{Sr}$ in enamel: biological turnover, enamel mineralization, and enamel sampling. First, the slow biological turnover of $^{87}\text{Sr}/^{86}\text{Sr}$ within the body is expected to attenuate $^{87}\text{Sr}/^{86}\text{Sr}$ intake³⁵, which is shown in Misha's tusk dentine³⁶. Second, with the expected damping and distortion of $^{87}\text{Sr}/^{86}\text{Sr}$ record due to enamel maturation, the next question is how maturation in different parts of the enamel attenuates the $^{87}\text{Sr}/^{86}\text{Sr}$ record. Since the innermost enamel layer adjacent to the enamel-dentine junction obtains a higher fraction of its mineral fraction from the secretion phase than the rest of the enamel^{37–39}, it is expected to exhibit a relatively unattenuated record of $^{87}\text{Sr}/^{86}\text{Sr}$ variations in the body^{23,40}. Lastly, if maturation influences the $^{87}\text{Sr}/^{86}\text{Sr}$ record in different ways within the enamel, how different sampling techniques further integrate the $^{87}\text{Sr}/^{86}\text{Sr}$ record becomes important, because they can affect our interpretation of measured enamel $^{87}\text{Sr}/^{86}\text{Sr}$. A detailed understanding of the relative contribution of these sources to the overall attenuation of $^{87}\text{Sr}/^{86}\text{Sr}$ intake/exposure can inform best practices in sampling, analysis, and data interpretation workflows.

To answer these questions, we employed a Sr-isotope mapping approach to examine $^{87}\text{Sr}/^{86}\text{Sr}$ within the molar plate using high-resolution in-situ LA-ICP-MS method (Fig. 1C). We used published data from Misha's tusk dentine³⁶ as a reference to benchmark our LA-ICP-MS $^{87}\text{Sr}/^{86}\text{Sr}$ data from the molar plate. To compare results from different sampling techniques, we also collected enamel samples using conventional drilling and micromilling (Fig. 1C and D) and analyzed them for $^{87}\text{Sr}/^{86}\text{Sr}$. We evaluated the influence of enamel maturation in each series using a Bayesian modeling framework. Lastly, we demonstrated an integrated microsampling (e.g., LA-ICP-MS) and modeling workflow, and discussed its utility in movement/

migration reconstructions and gaps in our knowledge with implications for future research.

Results

In-situ LA-ICP-MS analysis of Misha's Rm3.5 molar plate

A $^{87}\text{Sr}/^{86}\text{Sr}$ map of the molar enamel shows high-resolution spatial heterogeneity along both the crown to cervix axis and the enamel-dentine junction (EDJ) to the outer enamel surface (OES) axis (Fig. 2A). The major $^{87}\text{Sr}/^{86}\text{Sr}$ transitions (Change points 1 and 2, Fig. 2B) follow two parallel lines at an acute angle to the EDJ (Fig. 2B). For Enamel transects 1–8, the positions of both change points are consistent with the appositional angle (Fig. 2B). In contrast, in Enamel transects 9 and 10, closest to the OES, both change points are further from the EDJ than expected based on the appositional angle (Fig. 2B). Enamel transects 9 and 10 also show elevated $^{87}\text{Sr}/^{86}\text{Sr}$ values compared to the other transects (Supplementary Fig. 2).

Multi-substrate comparisons

To allow data comparisons between multiple substrates, we aligned the $^{87}\text{Sr}/^{86}\text{Sr}$ data series from molar enamel and tusk dentine (the reference) along the same time-axis using their incremental growth patterns (Methods, Supplementary Methods, Section 5). We found a remarkable agreement between the LA-ICP-MS $^{87}\text{Sr}/^{86}\text{Sr}$ time series of enamel transect 1 and micromilled tusk dentine $^{87}\text{Sr}/^{86}\text{Sr}$ data (Fig. 3A, B). Local variations in $^{87}\text{Sr}/^{86}\text{Sr}$ correspond well with that of the reference, with only a slight mismatch in the time axis (Fig. 3A, B). The LA-ICP-MS $^{87}\text{Sr}/^{86}\text{Sr}$ time series of enamel transects 9 and 10, conventionally drilled, and micromilled enamel $^{87}\text{Sr}/^{86}\text{Sr}$ series show slightly different patterns of turnover, especially with higher $^{87}\text{Sr}/^{86}\text{Sr}$ prior to the relocation and the smaller amplitudes of change than the reference (Fig. 3C–F, Supplementary Discussion 1 and 2, Supplementary Figs. 2 and 3).

Estimating the influence of enamel maturation

We evaluated the effects of enamel maturation using a model simulation of the fraction of post-relocation $^{87}\text{Sr}/^{86}\text{Sr}$ in each data series (Supplementary Methods, Section 6). We assumed that the elevated $^{87}\text{Sr}/^{86}\text{Sr}$ values observed in the pre-relocation data of some series are due to the inclusion of post-relocation Sr from Utah. For LA-ICP-MS transect 9 in the outer enamel, we estimated a small fraction of influence from enamel maturation, with a maximum a posteriori estimate (MAPE) of 0.06 (Fig. 3C, 89% credible

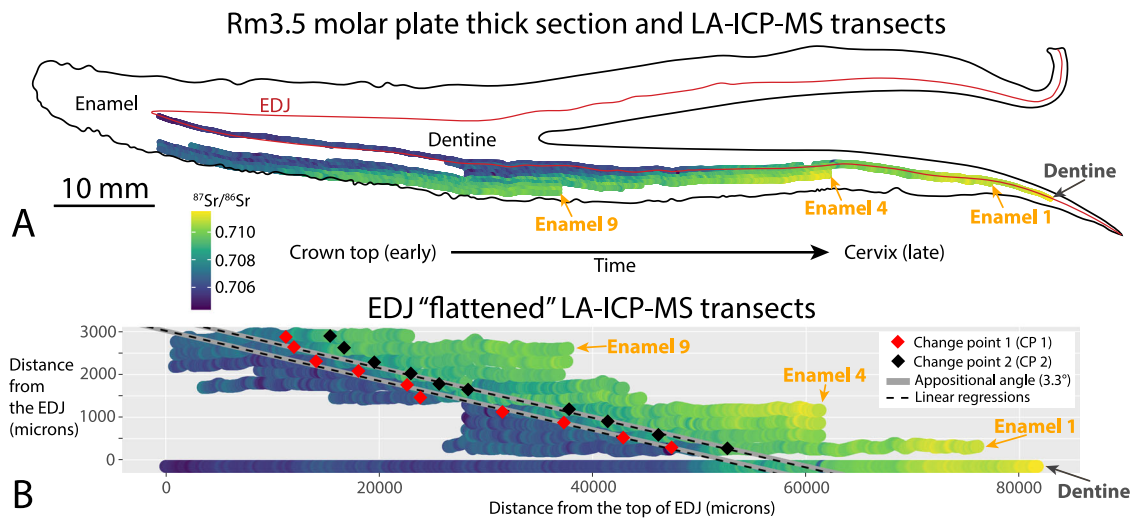


Fig. 2 | Summary of Laser Ablation Inductively Coupled Plasma Mass Spectrometry (LA-ICP-MS) results in reference to the geometry of Misha's Rm3.5 molar plate. **A** LA-ICP-MS transects mapped onto the molar plate. The red line marks the enamel-dentine junction (EDJ). Colored dots indicate LA-ICP-MS measured $^{87}\text{Sr}/^{86}\text{Sr}$ in dentine (dark gray arrow) and enamel (orange arrows). Cool colors indicate low $^{87}\text{Sr}/^{86}\text{Sr}$, while warm colors indicate high $^{87}\text{Sr}/^{86}\text{Sr}$. **B** LA-ICP-MS

transects accounting for the natural curvature of the molar plate (or EDJ "flattened") in the change point analysis. Change point 1 (CP 1, red diamond) marks the first abrupt rise in $^{87}\text{Sr}/^{86}\text{Sr}$ (fast turnover phase). Change point 2 (CP 2, black diamond) marks the subsequent gradual rise in $^{87}\text{Sr}/^{86}\text{Sr}$ (slow turnover phase). Linear trends of CP 1 and CP 2 (dashed lines), using Enamel transects 1–8, compared to the measured appositional angle (gray thick lines) of 3.3° .

interval or CI: 0.02 to 0.10, Supplementary Fig. 9). For LA-ICP-MS transect 10 in the outermost enamel, we estimated the fraction to be twice that of transect 9, with a MAPE of 0.13 (Fig. 3D, 89% CI: 0.09 to 0.17, Supplementary Fig. 9). For the conventionally drilled enamel samples, the fraction is the highest, with a MAPE of 0.23 (Fig. 3E, 89% CI: 0.18 to 0.29, Supplementary Fig. 9). For the micromilled enamel samples, we estimated a small fraction of influence from maturation, with a MAPE of 0.08 (Fig. 3F, 89% CI: 0.03 to 0.13, Supplementary Notes, Section 2, Supplementary Fig. 9). In addition, we noted that conventionally drilled $^{87}\text{Sr}/^{86}\text{Sr}$ tend to plot below the model simulations (Fig. 3E). Residual analysis shows a negative correlation between the residuals and the depths of the sampling grooves (Supplementary Fig. 10).

Discussion

The relocation history of Misha, with a unidirectional change in her $^{87}\text{Sr}/^{86}\text{Sr}$ intake (Fig. 1), permits a straightforward interpretation of isotope sampling transects from multiple substrates. For Misha's molar enamel, conventional drilling produces more attenuated $^{87}\text{Sr}/^{86}\text{Sr}$ data than does analysis of the tusk dentine and in-situ LA-ICP-MS, as reflected in the smaller magnitude of $^{87}\text{Sr}/^{86}\text{Sr}$ change and slightly slower transition from the pre- and post-relocation $^{87}\text{Sr}/^{86}\text{Sr}$ (Fig. 3). This can be explained by a combination of enamel maturation and the relatively large width of the sampling groove (~1 mm), both of which lead to time averaging (Supplementary Discussion 4 & 5). In addition, sampling depths can have a strong influence on the measured $^{87}\text{Sr}/^{86}\text{Sr}$ when the enamel $^{87}\text{Sr}/^{86}\text{Sr}$ is heterogeneous. Our samples were drilled at depths of ca. 1/3 of the enamel thickness, which explains the cervical offset in the measured position of the turnover event relative to LA-ICP-MS transect 10 close to the outer enamel surface (Supplementary Fig. 3). Drilling deeper into the enamel would shift the location of turnover towards the cervix by incorporating enamel that is formed earlier (with lower $^{87}\text{Sr}/^{86}\text{Sr}$ in this study) into the sample (Supplementary Notes, Section 2, Supplementary Discussions, Section 5). Finally, since sampling depths can be difficult to control during conventional drilling, they may introduce uncertainty to the measured $^{87}\text{Sr}/^{86}\text{Sr}$ when sampling across highly heterogeneous enamel. As such, conventional drilling is likely associated with uncertainties that are contingent on the underlying $^{87}\text{Sr}/^{86}\text{Sr}$ heterogeneity within the enamel, and we recommend prioritizing uniform drilling depths for studies that employ this method. The advantages of conventional drilling are ease of specimen preparation, less destructive

sampling, and high data accuracy and precision achievable using the solution method⁴¹.

The appositional geometry of $^{87}\text{Sr}/^{86}\text{Sr}$ turnover within the enamel (Fig. 2) makes micromilling that follows the same geometry a potential method to recover the primary $^{87}\text{Sr}/^{86}\text{Sr}$ turnover signal. However, $^{87}\text{Sr}/^{86}\text{Sr}$ values of the micromilled enamel samples show a temporally averaged turnover pattern with influence from post-relocation $^{87}\text{Sr}/^{86}\text{Sr}$, as well (Supplementary Discussion 2, Supplementary Fig. 3). This is likely due to our inability to set micromill paths that precisely follow the incremental growth features in the thick section used for sampling. We mapped the micromill paths as precisely as possible using measured appositional angles (Fig. 1C) relative to the curvature of the EDJ (Fig. 2A). In reality, the difference between the set micromill paths and the true incremental growth features may have grown larger as the micromill moves further along an individual path towards OES (Fig. 2B). $\delta^{13}\text{C}$ and $\delta^{18}\text{O}$ values of the same molar plate also show more abrupt changes in conventionally drilled samples than in micromilled samples²⁶, thus supporting our interpretation of time-averaging along each micromill sampling path. While micromilling has been successful in recovering a high-fidelity record of $^{87}\text{Sr}/^{86}\text{Sr}$ turnover in tusk dentine with a simple growth geometry^{6,36}, an improved milling geometry that precisely follows the enamel growth may be necessary to yield better results than in this study.

With the expected pattern of $^{87}\text{Sr}/^{86}\text{Sr}$ attenuation due to enamel maturation³², the $^{87}\text{Sr}/^{86}\text{Sr}$ value of Change point 1 can best inform the effect of overprint on the enamel Sr isotope composition during maturation (Supplementary Discussions, Section 4, Supplementary Fig. 7). Despite the prolonged enamel maturation process in elephants²⁶, the Change point 1 $^{87}\text{Sr}/^{86}\text{Sr}$ values of the LA-ICP-MS enamel transects are largely consistent with that of the reference (Supplementary Fig. 2), suggesting that most of the Sr within the inner half of Misha's enamel is deposited in the enamel secretion phase⁴². The geometry of the $^{87}\text{Sr}/^{86}\text{Sr}$ change points and its consistency with the appositional angle also support this interpretation (Fig. 2). This contrasts with results for carbon and oxygen isotopes in enamel and tusk dentine that suggest a larger influence of enamel maturation in these tracers (Supplementary Methods, Section 4, Supplementary Discussions Section 6). Enamel maturation effects on the $^{87}\text{Sr}/^{86}\text{Sr}$ of enamel seem to be more localized in the vicinity of the OES than is the case for carbon and oxygen (Supplementary Figs. 2 & 15). This can be explained by the OES-located ameloblasts during the maturation process⁴³: as mineral ions are

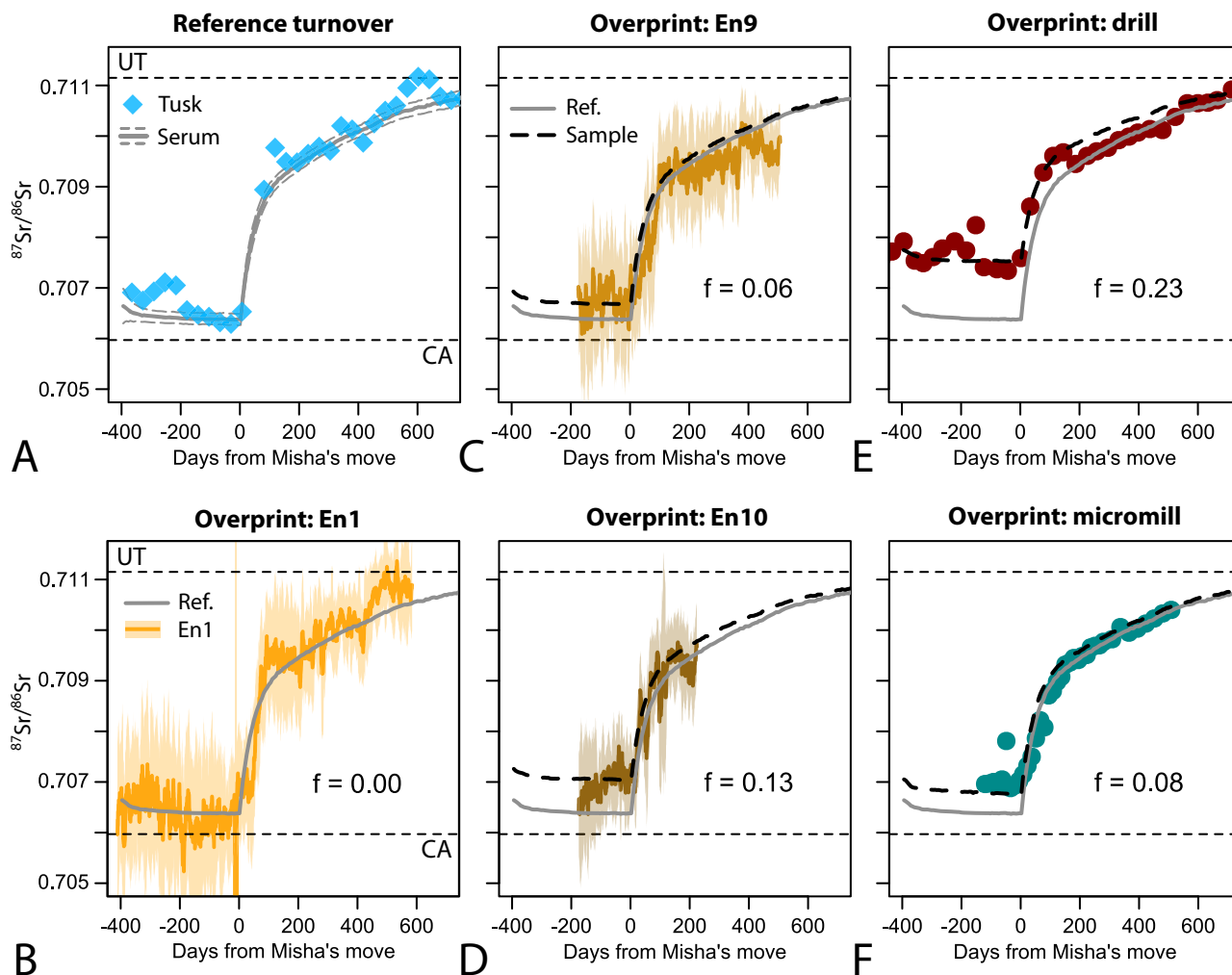


Fig. 3 | Estimated influence of enamel maturation (or overprint) in selected Laser Ablation Inductively Coupled Plasma Mass Spectrometry (LA-ICP-MS) generated $^{87}\text{Sr}/^{86}\text{Sr}$ enamel transects and conventionally drilled and micromilled enamel $^{87}\text{Sr}/^{86}\text{Sr}$ data series. Reconstructed $^{87}\text{Sr}/^{86}\text{Sr}$ turnover timelines among micromilled tusk dentine (A, light blue diamonds, Supplementary Table 1), LA-ICP-MS molar enamel (B–D, 25-point mean as orange lines with standard deviations as shadings, Supplementary Fig. 2), molar enamel with conventional drilling (E, red

dots), and molar enamel with micromilling (F, turquoise dots). Simulated serum $^{87}\text{Sr}/^{86}\text{Sr}$ timeline (A, gray thick curve with dashed bracketing) is used as the reference (B–F, Ref., gray thick curves). Simulated sample $^{87}\text{Sr}/^{86}\text{Sr}$ timeline with influence from maturation (C–F, Sample, black dashed curves) is used to estimate the fractional influence as “f” (displaying maximum a posteriori estimates or MAPE, Supplementary Fig. 9) in each panel. Horizontal dashed lines indicate the presumed $^{87}\text{Sr}/^{86}\text{Sr}$ sources of California (CA) and Utah (UT).

transported to the OES⁴⁴, Sr diffuses into the enamel matrix through the OES with more difficulty than bicarbonate, thus creating a more localized effect near the OES. Enamel transect 10 is still *ca.* 300 microns from the OES (Fig. 2), and projecting the relationship observed in the transects to the OES, we expect that the maturation overprint at the OES would be even larger than that seen in the conventionally drilled samples ($f=0.23$). In Misha’s molar, the thick enamel (*ca.* 3 mm) likely limits the impact of this process to locations in close proximity to the OES. In taxa with thinner enamel (e.g., in *Elephas* or *Mammuthus primigenius*, both about half of Misha’s enamel thickness) the influence of maturation may reach proportionally deeper into inner enamel⁴⁰. As such, sampling strategies that include the outer enamel (e.g., conventional drilling) may produce smaller amplitudes of $^{87}\text{Sr}/^{86}\text{Sr}$ change than the primary $^{87}\text{Sr}/^{86}\text{Sr}$ turnover series due to enamel maturation.

One way to potentially minimize the influence of maturation is to remove the outer enamel layer or specifically target the innermost enamel⁴⁵. To explore the theoretical efficacy of such sampling strategies, we used a forward modeling framework with synthetic $^{87}\text{Sr}/^{86}\text{Sr}$ intake histories, simulated enamel appositional geometry and $^{87}\text{Sr}/^{86}\text{Sr}$, and sampling geometries that aggregate the heterogeneous $^{87}\text{Sr}/^{86}\text{Sr}$ within the sampling groove (Supplementary Discussions, Section 5). We found that

conventional drilling not only tends to produce temporally averaged $^{87}\text{Sr}/^{86}\text{Sr}$ series than the primary $^{87}\text{Sr}/^{86}\text{Sr}$ turnover due to sample averaging, but also series with notable timeline shifts due to the underlying $^{87}\text{Sr}/^{86}\text{Sr}$ heterogeneity within the enamel (Supplementary Table 7, Supplementary Fig. 14). These issues suggest exercising caution when interpreting results from conventional drilling, as they may bias reconstructions of movement history⁴⁶. In comparison, sampling the innermost *ca.* 0.2 mm of enamel can potentially recover a near-complete $^{87}\text{Sr}/^{86}\text{Sr}$ amplitude as in the primary turnover, thus minimizing the influence of both enamel maturation and sample averaging (Supplementary Fig. 14).

While signal attenuation due to enamel maturation can be minimized by microsampling techniques that target the innermost enamel, the slow $^{87}\text{Sr}/^{86}\text{Sr}$ turnover within the body is still the primary source of input signal attenuation. Therefore, we recommend an integrated microsampling and modeling workflow that can facilitate geospatially explicit interpretations of seasonal migration. We demonstrate how inverse modeling can account for $^{87}\text{Sr}/^{86}\text{Sr}$ turnover, by extending the BITS model³⁶ to Misha’s LA-ICP-MS enamel data and micromilled tusk dentine data (Fig. 4, Supplementary Material Section 1, Supplementary Data 2 & 3). BITS, or the Bayesian Isotope Turnover and Sampling model, was originally developed to provide

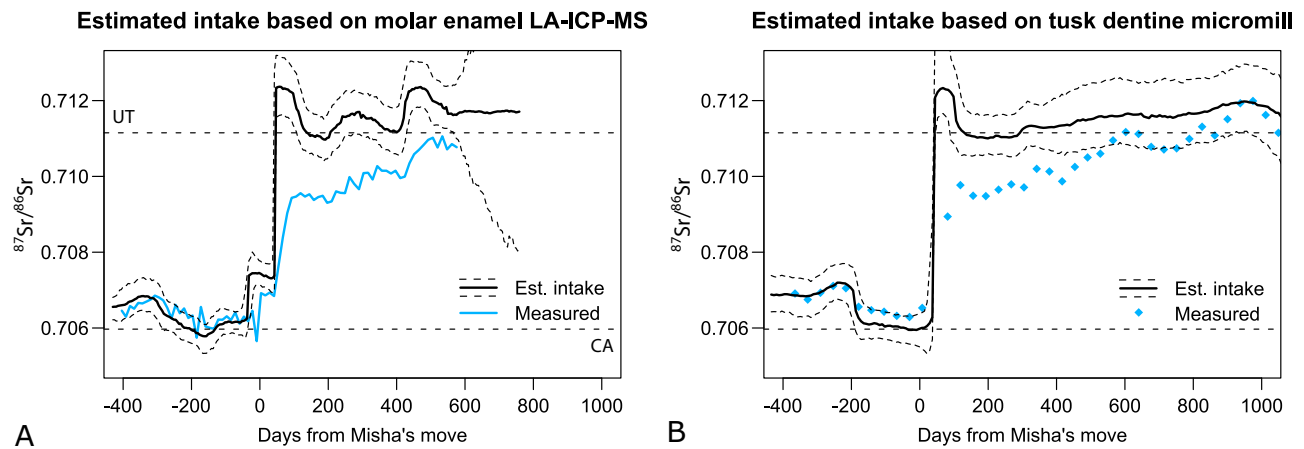


Fig. 4 | Comparison between the estimated $^{87}\text{Sr}/^{86}\text{Sr}$ intake series from Laser Ablation Inductively Coupled Plasma Mass Spectrometry (LA-ICP-MS) of Misha's molar enamel (Enamel transect 1) and micromilled tusk dentine, using the Bayesian Isotope Turnover and Sampling (BITS) framework³⁶. The black

thick line represents the Maximum a posteriori estimates of the $^{87}\text{Sr}/^{86}\text{Sr}$ intake, while the dashed lines represent the 89% highest density intervals. The blue line (A) represents the 50-point averaged LA-ICP-MS $^{87}\text{Sr}/^{86}\text{Sr}$ series. The blue diamonds (B) are the micromilled tusk dentine $^{87}\text{Sr}/^{86}\text{Sr}$ series.

quantitative $^{87}\text{Sr}/^{86}\text{Sr}$ reconstructions from LA-ICP-MS $^{87}\text{Sr}/^{86}\text{Sr}$ profiles in proboscidean tusks³⁶. Here, we improved the model framework with customized dental growth rates and reduced computational demands (Supplementary Discussions, Section 7). The independently estimated $^{87}\text{Sr}/^{86}\text{Sr}$ intake histories are consistent with Misha's relocation, both in the $^{87}\text{Sr}/^{86}\text{Sr}$ amplitude of change and the timing of the relocation (Methods, Fig. 4). Despite some differences in the posterior estimates of some model parameters for the two series, the estimated $^{87}\text{Sr}/^{86}\text{Sr}$ intake series derived from the two substrates are almost identical (Fig. 4, Supplementary Fig. 16). The large $^{87}\text{Sr}/^{86}\text{Sr}$ gaps between the estimated $^{87}\text{Sr}/^{86}\text{Sr}$ intake histories and the intra-tooth results suggest that inverse modeling can support more robust interpretation of intra-tooth $^{87}\text{Sr}/^{86}\text{Sr}$ data than conventional approaches. The small local variations estimated from the LA-ICP-MS series are likely due to its higher data resolution than that of the tusk dentine (Supplementary Discussions, Section 7). Overall, the combination of micro-sampling (such as LA-ICP-MS) followed by inverse modeling is a promising workflow for quantitative movement/migration reconstructions. With this workflow, the resultant $^{87}\text{Sr}/^{86}\text{Sr}$ intake series can be coupled with movement models, isoscapes, and statistical tools to make geospatially explicit reconstructions of animal movement and migration patterns^{7,22,47}.

The demonstrated microsampling and modeling workflow has tremendous potential in answering a wide range of questions in forensic science, archeology, paleontology, and conservation biology. The workflow allows in-situ analysis of small dental elements such as modern or ancient human teeth to study movement histories of target individuals or populations^{48,49}, as well as life history events, subsistence strategies, cultural practices, and social structures of past societies^{50–52}. When applied to domesticated animals and coupled with additional isotopic tracers (e.g., $\delta^{13}\text{C}$ and $\delta^{18}\text{O}$), the workflow can potentially inform strategies of animal husbandry such as seasonal residence regions, trade, and the timing of migration^{53–55}. The minimally destructive LA-ICP-MS method can also be applied to fossil hominin tooth fragments to study their landscape use and make inferences on their social or reproductive characteristics⁵⁶. Lastly, movement and migration patterns of the past can help us understand how migrations evolved over time⁵⁷, and how migrations of endangered animals have been disrupted by human activities, guiding our future conservation efforts^{58,59}.

With the recent growth in the application of Sr isotopes to studies of mobility, gaps in our knowledge became more visible. For example, while we estimated the fraction of the post-movement $^{87}\text{Sr}/^{86}\text{Sr}$ in selected data series (Fig. 3, Supplementary Methods 6), we were unable to evaluate the timing or the extent of the influence of maturation for $^{87}\text{Sr}/^{86}\text{Sr}$, as in studies of enamel mineral density^{30,32}. A controlled feeding experiment on a model organism

in multiple cohorts raised to different ontogenetic stages would be ideal to investigate the extent and duration of the maturation process⁶⁰. Studies on modern animals provide the most fundamental understanding of how strontium and other isotope tracers are archived in mineralized tissues, and how such records can be used to inform their biology²⁴. While the $^{87}\text{Sr}/^{86}\text{Sr}$ turnover parameters in a captive elephant provide an excellent start, similar work needs to be done on wild individuals and in other species to provide confidence for broader applications of the workflow. With carefully designed experimental and modeling approaches, future studies can test and validate the workflow for more robust estimations of intake histories of $^{87}\text{Sr}/^{86}\text{Sr}$ and other isotope tracers from molar enamel. Doing so can ultimately improve our interpretation of movement/migration or other life history patterns.

In conclusion, studies of modern animals can provide a fundamental understanding of how strontium isotopes ($^{87}\text{Sr}/^{86}\text{Sr}$) are archived in mineralized tissues, and how we use such records to reconstruct animal or human mobility. Our study addressed two major challenges associated with interpreting movement/migration patterns from $^{87}\text{Sr}/^{86}\text{Sr}$ in dental tissues. The first was evaluating the relative influence of three sources of $^{87}\text{Sr}/^{86}\text{Sr}$ signal attenuation in enamel: biological turnover, maturation, and sampling. The second was recovering the primary $^{87}\text{Sr}/^{86}\text{Sr}$ input signal from different dental tissues. We showed that microsampling can minimize the influence of maturation and sampling, but inverse modeling is essential to account for attenuation associated with Sr turnover. Our demonstrated microsampling-modeling workflow can support robust interpretations of animal and human migration patterns in forensic science, archeology, paleontology, and conservation biology.

Methods

Life history of Misha and experimental settings

Misha was a female African savanna elephant (*Loxodonta africana*) captured in South Africa at about 1 year old in 1982. She was soon transferred to the Happy Hollow Zoo in San José, California, and again in 1983 to Marine World Africa in Redwood Shores, California, and again in 1986 to Six Flags Discovery Kingdom in Vallejo, California, where she stayed for nearly 20 years. On April 22, 2005, Misha was relocated to Utah's Hogle Zoo in Salt Lake City. On September 9, 2008, after ca. 3.5 years of residence in Utah, Misha was euthanized due to rapidly declining health at about 27 years old²⁶. At the Hogle Zoo, she was provided *ad libitum* with commercial elephant pellets, herbivore mineral supplements, dry hay produced in the Cache Valley, Utah, and water from the municipal supply. With $^{87}\text{Sr}/^{86}\text{Sr}$ measured in her feed and water, dry hay was likely her primary source of Sr intake based on her post-relocation $^{87}\text{Sr}/^{86}\text{Sr}$ at ca. 0.71115³⁶. While no food or

water samples are available from her residency in Vallejo, California, her pre-relocation $^{87}\text{Sr}/^{86}\text{Sr}$ of tusk dentine was stable, at *ca.* 0.7065 (Fig. 3A)³⁶.

Material preparation and sampling

Misha's lower right third molar had not erupted at death. The mesial four molar plates were fully mineralized with cementum covering the entire crown section. The fifth plate (Rm3.5) was not entirely mineralized (Supplementary Note 1), with enamel and dentine formation fronts visible at the cervix of the plate (Fig. 1C). We cut the Rm3.5 plate along the mid-sagittal plane into three pieces. We left the lingual piece intact. We cut the middle piece (~5 mm thick) into three blocks (coronal, middle, and cervical) so that each can fit the dimensions of a standard petrographic slide to produce enamel growth and mineralization data²⁶. We sampled the middle piece with conventional drilling and micromilling techniques, with the resulting powder used for $^{87}\text{Sr}/^{86}\text{Sr}$ analysis (more details below) and stable carbon and oxygen isotope analysis (Supplementary Methods 4)²⁶. We prepared the buccal piece into a thick section by embedding it in transparent epoxy resin before cutting it free with a precision saw (Buehler – Isomet Low Speed) and an Isomet Diamond Wafering Blade (102 × 0.3 mm). The cut resulted in a section at *ca.* 3.8 mm thickness. We ground down the freshly cut surface to *ca.* 3.5 mm thickness, using a rotary polisher with abrasive paper at 400 grit, then polished with successive finer grits to 1600 grit. We scanned the thick section (*ca.* 100 mm by 25 mm) in color at 9600 dpi using an Epson® 4490 Photo flatbed scanner (Fig. 1C) and mounted it directly in the laser chamber for subsequent *in situ* LA-ICP-MS analysis.

We removed the cementum from the middle piece of the Rm3.5 plate before conventional drilling and micromilling. We first collected conventional hand drilled enamel samples from the lingual side of middle piece of the Rm3.5 plate along its entire length (Fig. 1C), using a low-speed rotary tool with a 1 mm diamond drill bit. The serial sampling grooves are *ca.* 3 mm in length, perpendicular to the growth axis of the tooth at *ca.* 2 mm intervals between the grooves, and between 0.5 to 1.2 mm deep (Fig. 1C, Supplementary code “data/Rm3.5 hand drill.csv”)²⁶. After cutting the middle piece into three blocks, we then collected micromilled enamel samples from the buccal side of the middle block (Fig. 1C) at 1 mm depth with 50-micron intervals from the OES to the EDJ. We milled the outermost nine samples at 100-micron intervals to produce enough powder for analyses because of shorter effective milling paths and less dense enamel. We set the micromill paths at 3.3 degrees to the EDJ, following the appositional angle of the enamel²⁶.

$^{87}\text{Sr}/^{86}\text{Sr}$ analyses

We conducted the LA-ICP-MS analyses on the distal side of the Rm3.5 thick section (Fig. 1C). The apposition of the molar enamel starts at the crown end following an acute angle to the EDJ and continues towards the cervix²⁶. Therefore, older enamel is located on the crown side along the EDJ, and on the EDJ side across the thickness of the enamel. We analyzed 10 enamel transects, covering the majority of the Rm3.5 molar plate (Fig. 2B). We placed the first enamel transect (Enamel 1) *ca.* 150 microns to the EDJ, and subsequent transects parallel to the EDJ at 300-micron increment towards the OES (Fig. 2). We started each transect from the crown end, following enamel growth longitudinally towards the cervix. Because the natural curvature of the molar plate may influence $^{87}\text{Sr}/^{86}\text{Sr}$ turnover geometry, we analyzed one dentine transect 150 microns to the EDJ (Fig. 2B, dentine) to facilitate evaluation of the geometry. We transformed the original laser positions of the enamel transects so that the EDJ is “flattened” referencing the dentine transect (Supplementary Discussion 1). The coordinate transformation produces enamel transects that are almost parallel to the EDJ (Fig. 2B), which reduces the influences of the tooth's curvature when evaluating the $^{87}\text{Sr}/^{86}\text{Sr}$ turnover geometry within the enamel.

We carried out the LA-ICP-MS $^{87}\text{Sr}/^{86}\text{Sr}$ analysis using standard laser settings with blank and major element ratio corrections (Supplementary Methods 2, Supplementary Table 2). Due to the isobaric interference of $^{40}\text{Ca}^{31}\text{P}^{16}\text{O}^{61,62}$, we corrected the LA-ICP-MS $^{87}\text{Sr}/^{86}\text{Sr}$ results using published

equations (Supplementary Methods 2). Due to the high data density and level of noise (standard deviation ~ 0.001), we calculated a 25-point moving average and standard deviation for the corrected $^{87}\text{Sr}/^{86}\text{Sr}$ (Supplementary Data 1, Supplementary code “01 Helper fx.R”). We mapped the $^{87}\text{Sr}/^{86}\text{Sr}$ moving averages onto the Rm3.5 molar plate by interpolating the ICP-MS time stamps using the timed laser positions grid (Fig. 2A, Supplementary Data 1, Supplementary code “01 Helper fx.R”, and “02 Data processing.R”). We compared the LA-ICP-MS $^{87}\text{Sr}/^{86}\text{Sr}$ results with those of micromilled tusk dentine samples (Supplementary Methods 1, Supplementary Fig. 1) using the solution method with standard protocols to ensure the accuracy of the LA-ICP-MS data (Supplementary Methods 3). Conventionally drilled and micromilled enamel samples from the Rm3.5 molar plate (Fig. 1C) were also analyzed using the solution method.

Comparisons of $^{87}\text{Sr}/^{86}\text{Sr}$ turnover among different data series

To reference different $^{87}\text{Sr}/^{86}\text{Sr}$ series to the same time dimension, we performed timeline reconstructions³⁴ using growth rate estimates and intra-tooth sampling distance measurements (Supplementary Methods 5). The growth increments of Misha's Rm3.5 plate show that the average enamel extension rate is 55.3 microns per day²⁶. For enamel growth, we assumed that the extension rate scales with the appositional angle that follows a logarithmic trend along the length of the molar (Supplementary Fig. 4, Supplementary code “04 timeline reconstruction.R”). We then used the growth-length relationship to reconstruct timelines for all $^{87}\text{Sr}/^{86}\text{Sr}$ data series sampled along the Rm3.5 molar plate (Fig. 3, Supplementary code “04 timeline reconstruction.R”). We assumed that Misha's tusk dentine was growing at 14.7 microns per day radially²⁶, with the equivalent sampling interval at 547 microns (Supplementary Fig. 1). We calculated the time interval between each pair of sampling locations, and the total time elapses using a cumulative function (Supplementary Methods 5, Supplementary Fig. 5). Lastly, we matched the different timelines by manually aligning the first abrupt increase in each $^{87}\text{Sr}/^{86}\text{Sr}$ turnover curve, corresponding to the date of Misha's relocation event (Fig. 3).

Statistics and Modeling

To evaluate the geometry of the $^{87}\text{Sr}/^{86}\text{Sr}$ turnover within the enamel, within each LA-ICP-MS transect, we used segmented linear regressions⁶³ to detect major $^{87}\text{Sr}/^{86}\text{Sr}$ change points (Fig. 2B, Supplementary Discussion 1, Supplementary Fig. 2). We mapped out the two change points along the coordinate transformed transects (Fig. 2B) and compared their locations to the enamel appositional geometry (Fig. 2C, Supplementary Discussion 1, Supplementary Fig. 2, Supplementary code “03 Change point analysis.R”). To estimate the effect of enamel maturation, we used a Bayesian modeling approach based on the BITS framework (Supplementary Methods 6). We used a linear mixing process between the overturning serum $^{87}\text{Sr}/^{86}\text{Sr}$ and the post-movement $^{87}\text{Sr}/^{86}\text{Sr}$ to estimate the fractional influence of enamel maturation for four $^{87}\text{Sr}/^{86}\text{Sr}$ data series (Fig. 3, Supplementary Methods 6, Supplementary code “05 Overprint estimation.R”). To demonstrate the recommended microsampling-modeling workflow of estimating $^{87}\text{Sr}/^{86}\text{Sr}$ intake from different dental tissues, we apply the BITS Bayesian model framework to Misha's LA-ICP-MS of molar enamel and micromilled tusk dentine $^{87}\text{Sr}/^{86}\text{Sr}$ data (Supplementary Discussion 7). We implemented the two modeling approaches in R using the “R2jags” package⁶⁴ with the standalone JAGS (Just Another Gibbs Sampler) encoder installed separately⁶⁵. We adjusted the model parameters based on a series of sensitivity tests (Supplementary Note 3, Supplementary Table 3, Supplementary Figs. 8, 11, 12, 16). We carried out the above statistical analyses in RStudio using R version 4.3.1⁶⁶. We also applied the reaction progress framework (Supplementary Table 8)^{67,68} to Misha's micromilled tusk dentine $^{87}\text{Sr}/^{86}\text{Sr}$ data as an approach to account for the biological turnover of $^{87}\text{Sr}/^{86}\text{Sr}$ (Supplementary Discussion 8, Supplementary Fig. 17, Supplementary Data 4).

Reporting summary

Further information on research design is available in the Nature Portfolio Reporting Summary linked to this article.

Data availability

The compiled data files (Supplementary Data 1–4), LA-ICP-MS raw data files, custom code with model scripts used to generate the figures that support the findings of this study are available in Zenodo with the identifier <https://doi.org/10.5281/zenodo.12511048>⁶⁹.

Code availability

Custom code with model scripts used to generate the figures that support the findings of this study are available in Zenodo with the identifier <https://doi.org/10.5281/zenodo.12511048>⁶⁹.

Received: 29 September 2024; Accepted: 5 February 2025;

Published online: 21 February 2025

References

- Dietl, G. P. et al. Conservation paleobiology: leveraging knowledge of the past to inform conservation and restoration. *Annu. Rev. Earth Planet. Sci.* **43**, 79–103 (2015).
- Pringle, R. M. et al. Impacts of large herbivores on terrestrial ecosystems. *Curr. Biol.* **33**, R584–R610 (2023).
- Koch, P. L., Fisher, D. C. & Dettman, D. Oxygen isotope variation in the tusks of extinct proboscideans: A measure of season of death and seasonality. *Geology* **17**, 515–519 (1989).
- Bocherens, H., Fizet, M., Mariotti, A., Gangloff, R. A. & Burns, J. A. Contribution of isotopic biogeochemistry (¹³C, ¹⁵N, ¹⁸O) to the paleoecology of mammoths (*Mammuthus primigenius*). *Hist. Biol.* **7**, 187–202 (1994).
- Cherney, M. D. et al. Testosterone histories from tusks reveal woolly mammoth musth episodes. *Nature* **618**, E22 (2023).
- Miller, J. H., Fisher, D. C., Crowley, B. E., Secord, R. & Konomi, B. A. Male mastodon landscape use changed with maturation (late Pleistocene, North America). *Proc. Natl Acad. Sci.* **119**, e2118329119 (2022).
- Wooller, M. J. et al. Lifetime mobility of an Arctic woolly mammoth. *Science* **373**, 806–808 (2021).
- Fisher, D. C. Paleobiology of Pleistocene Proboscideans. *Annu. Rev. Earth Planet. Sci.* **46**, 229–260 (2018).
- Dirks, W., Bromage, T. G. & Agenbroad, L. D. The duration and rate of molar plate formation in *Palaeoloxodon cypristes* and *Mammuthus columbi* from dental histology. *Quat. Int.* **255**, 79–85 (2012).
- Fisher, D. C. & Fox, D. L. in *From the Dent Prairie to the Peaks of the Rockies: Recent Paleoindian Research in Colorado* (eds R. H. Brunswig & B. L. Pitblado) 123–153 (University of Colorado Press, 2007).
- Britton, K. et al. Sampling plants and malacofauna in ⁸⁷Sr/⁸⁶Sr bioavailability studies: implications for isoscape mapping and reconstructing of past mobility patterns. *Front. Ecol. Evol.* **8**, 579473 (2020).
- Crowley, B. E., Miller, J. H. & Bataille, C. P. Strontium isotopes (⁸⁷Sr/⁸⁶Sr) in terrestrial ecological and palaeoecological research: empirical efforts and recent advances in continental-scale models. *Biol. Rev.* **92**, 43–59 (2017).
- Makarewicz, C. A. & Sealy, J. Dietary reconstruction, mobility, and the analysis of ancient skeletal tissues: Expanding the prospects of stable isotope research in archaeology. *J. Archaeol. Sci.* **56**, 146–158 (2015).
- Holt, E., Evans, J. A. & Madgwick, R. Strontium (⁸⁷Sr/⁸⁶Sr) mapping: a critical review of methods and approaches. *Earth-Sci. Rev.* **216**, 103593 (2021).
- Coelho, I., Castanheira, I., Bordado, J. M., Donard, O. & Silva, J. A. L. Recent developments and trends in the application of strontium and its isotopes in biological related fields. *TrAC Trends Anal. Chem.* **90**, 45–61 (2017).
- Sillen, A. & Kavanagh, M. Strontium and paleodietary research: a review. *Am. J. Phys. Anthropol.* **25**, 67–90 (1982).
- Bataille, C. P., Crowley, B. E., Wooller, M. J. & Bowen, G. J. Advances in global bioavailable strontium isoscapes. *Palaeogeogr. Palaeoclimatol. Palaeoecol.* **555**, 109849 (2020).
- Lewis, J., Pike, A. W. G., Coath, C. D. & Evershed, R. P. Strontium concentration, radiogenic (⁸⁷Sr/⁸⁶Sr) and stable (⁸⁸Sr) strontium isotope systematics in a controlled feeding study. *STAR: Sci. Technol. Archaeol. Res.* **3**, 45–57 (2017).
- Anders, D., Osmanovic, A. & Vohberger, M. Intra- and inter-individual variability of stable strontium isotope ratios in hard and soft body tissues of pigs. *Rapid Commun. Mass Spectrom.* **33**, 281–290 (2019).
- Wunder, M. B. in *Isoscapes: Understanding Movement, Pattern, and Process on Earth through Isotope Mapping* (eds Jason et al.) 251–270 (Springer Netherlands, 2010).
- Bowen, G. J. & West, J. B. in *Terrestrial Ecology* (eds Hobson, K. A. & Wassenaar, L. I.) Vol. 2, 79–105 (Elsevier, 2008).
- Rowe, A. G. et al. A female woolly mammoth's lifetime movements end in an ancient Alaskan hunter-gatherer camp. *Sci. Adv.* **10**, eadk0818 (2024).
- Kowalik, N. et al. Revealing seasonal woolly mammoth migration with spatially-resolved trace element, Sr and O isotopic records of molar enamel. *Quat. Sci. Rev.* **306**, 108036 (2023).
- Koch, P. L. in *Stable Isotopes in Ecology and Environmental Science* (eds Michener, R. & Lajtha, K.) 99–154 (Wiley, 2007).
- Martínez del Río, C., Wolf, N., Carleton, S. A. & Gannes, L. Z. Isotopic ecology ten years after a call for more laboratory experiments. *Biol. Rev.* **84**, 91–111 (2009).
- Uno, K. T. et al. Forward and inverse methods for extracting climate and diet information from stable isotope profiles in proboscidean molars. *Quat. Int.* **557**, 92–109 (2020).
- Uno, K. T. et al. High-resolution stable isotope profiles of modern elephant (*Loxodonta africana*) tusk dentin and tail hair from Kenya: Implications for identifying seasonal variability in climate, ecology, and diet in ancient proboscideans. *Palaeogeogr. Palaeoclimatol. Palaeoecol.* **559**, 109962 (2020).
- Budd, P., Montgomery, J., Barreiro, B. & Thomas, R. G. Differential diagenesis of strontium in archaeological human dental tissues. *Appl. Geochem.* **15**, 687–694 (2000).
- Weber, K. et al. Diagenetic stability of non-traditional stable isotope systems (Ca, Sr, Mg, Zn) in teeth—an in-vitro alteration experiment of biogenic apatite in isotopically enriched tracer solution. *Chem. Geol.* **572**, 120196 (2021).
- Green, D. R. et al. Synchrotron imaging and Markov Chain Monte Carlo reveal tooth mineralization patterns. *PLoS ONE* **12**, e0186391 (2017).
- Suga, S. Progressive mineralization pattern of developing enamel during the maturation stage. *J. Dent. Res.* **61**, 1532–1542 (1982).
- Passey, B. H. & Cerling, T. E. Tooth enamel mineralization in ungulates: implications for recovering a primary isotopic time-series. *Geochim. Cosmochim. Acta* **66**, 3225–3234 (2002).
- Green, D. R. et al. Quantitative reconstruction of seasonality from stable isotopes in teeth. *Geochim. Cosmochim. Acta* **235**, 483–504 (2018).
- Yang, D. et al. Intra-tooth stable isotope profiles in warthog canines and third molars: Implications for paleoenvironmental reconstructions. *Chem. Geol.* **554**, 119799 (2020).
- Montgomery, J., Evans, J. A. & Horstwood, M. S. A. Evidence for long-term averaging of strontium in bovine enamel using TIMS and LA-MC-ICP-MS strontium isotope intra-molar profiles. *Environ. Archaeol.* **15**, 32–42 (2010).
- Yang, D. et al. BITS: A Bayesian Isotope Turnover and Sampling model for strontium isotopes in proboscideans and its potential utility in movement ecology. *Methods Ecol. Evol.* **14**, 2800–2813 (2023).
- Blumenthal, S. A. et al. Stable isotope time-series in mammalian teeth: In situ ^δ¹⁸O from the innermost enamel layer. *Geochim. Cosmochim. Acta* **124**, 223–236 (2014).

38. Allan, J. H. Investigations into the mineralization pattern of human dental enamel. *J. Dent. Res.* **38**, 1096–1107 (1959).
39. Tafforeau, P., Bentaieb, I., Jaeger, J.-J. & Martin, C. Nature of laminations and mineralization in rhinoceros enamel using histology and X-ray synchrotron microtomography: Potential implications for palaeoenvironmental isotopic studies. *Palaeogeogr. Palaeoclimatol. Palaeoecol.* **246**, 206–227 (2007).
40. Anczkiewicz, R. et al. High spatial resolution Sr isotope and trace element record of dental enamel mineralization in a woolly mammoth tooth: Implications for paleoecological reconstructions. *Quat. Sci. Rev.* **313**, 108191 (2023).
41. Simonetti, A., Buzon, M. R. & Creaser, R. A. In-situ elemental and Sr isotope investigation of human tooth enamel by laser ablation-(MC)-ICP-MS: Successes and pitfalls. *Archaeometry* **50**, 371–385 (2008).
42. Dean, M. C., Le Cabec, A., Van Malderen, S. J. M. & Garrevoet, J. Synchrotron X-ray fluorescence imaging of strontium incorporated into the enamel and dentine of wild-shot orangutan canine teeth. *Arch. Oral Biol.* **119**, 104879 (2020).
43. Simmer, J. P. & Fincham, A. G. Molecular mechanisms of dental enamel formation. *Crit. Rev. Oral Biol. Med.* **6**, 84–108 (1995).
44. Bronckers, A. L. J. J. Ion transport by ameloblasts during amelogenesis. *J. Dent. Res.* **96**, 243–253 (2017).
45. Widga, C. et al. Life histories and niche dynamics in late Quaternary proboscideans from midwestern North America. *Quat. Res.* **100**, 224–239 (2021).
46. Le Corre, M., Grimes, V., Lam, R. & Britton, K. Comparison between strip sampling and laser ablation methods to infer seasonal movements from intra-tooth strontium isotopes profiles in migratory caribou. *Sci. Rep.* **13**, 3621 (2023).
47. Ma, C., Vander Zanden, H. B., Wunder, M. B. & Bowen, G. J. assignR: An R package for isotope-based geographic assignment. *Methods Ecol. Evol.* **11**, 996–1001 (2020).
48. Richards, M. et al. Strontium isotope evidence of Neanderthal mobility at the site of Lakonis, Greece using laser-ablation PIMMS. *J. Archaeol. Sci.* **35**, 1251–1256 (2008).
49. Müller, W. et al. Enamel mineralization and compositional time-resolution in human teeth evaluated via histologically-defined LA-ICPMS profiles. *Geochim Cosmochim. Acta* **255**, 105–126 (2019).
50. Guede, I. et al. Analyses of human dentine and tooth enamel by laser ablation-inductively coupled plasma-mass spectrometry (LA-ICP-MS) to study the diet of medieval Muslim individuals from Tauste (Spain). *Microchem. J.* **130**, 287–294 (2017).
51. Coffin, J., Dolphin, A. E., Jackes, M., Yakymchuk, C. & Perrin, T. Exploring childhood mobility in Neolithic Southern France (Roquemissou) using incremental analyses of Sr isotope ratios in tooth enamel. *J. Archaeol. Sci.: Rep.* **42**, 103417 (2022).
52. Kowalik, N. et al. Tracing human mobility in central Europe during the Upper Paleolithic using sub-seasonally resolved Sr isotope records in ornaments. *Sci. Rep.* **10**, 10386 (2020).
53. Chakraborty, K. S. et al. Enamel isotopic data from the domesticated animals at Kotada Bhadli, Gujarat, reveals specialized animal husbandry during the Indus Civilization. *J. Archaeol. Sci.: Rep.* **21**, 183–199 (2018).
54. Chazin, H., Gordon, G. W. & Knudson, K. J. Isotopic perspectives on pastoralist mobility in the Late Bronze Age South Caucasus. *J. Anthropol. Archaeol.* **54**, 48–67 (2019).
55. Pryor, A. J. E. et al. Isotopic biographies reveal horse rearing and trading networks in medieval London. *Sci. Adv.* **10**, ead5782 (2024).
56. Hamilton, M. I., Copeland, S. R. & Nelson, S. V. A reanalysis of strontium isotope ratios as indicators of dispersal in South African hominins. *J. Hum. Evol.* **187**, 103480 (2024).
57. O'Brien, K. et al. Limited herbivore migration during the Last Glacial Period of Kenya. *Nat. Ecol. Evol.* **8**, 1191–1198 (2024).
58. Doherty, T. S., Hays, G. C. & Driscoll, D. A. Human disturbance causes widespread disruption of animal movement. *Nat. Ecol. Evol.* **5**, 513–519 (2021).
59. Kauffman, M. J. et al. Causes, consequences, and conservation of ungulate migration. *Annu. Rev. Ecol. Evol. Syst.* **52**, 453–478 (2021).
60. Weber, M. et al. Strontium uptake and intra-population $^{87}\text{Sr}/^{86}\text{Sr}$ variability of bones and teeth—controlled feeding experiments with rodents (*Rattus norvegicus*, *Cavia porcellus*). *Front. Ecol. Evol.* **8**, <https://doi.org/10.3389/fevo.2020.569940> (2020).
61. Lewis, J., Coath, C. & Pike, A. An improved protocol for $^{87}\text{Sr}/^{86}\text{Sr}$ by laser ablation multi-collector inductively coupled plasma mass spectrometry using oxide reduction and a customised plasma interface. *Chem. Geol.* **390**, 173–181 (2014).
62. Irrgeher, J., Galler, P. & Prohaska, T. $^{87}\text{Sr}/^{86}\text{Sr}$ isotope ratio measurements by laser ablation multicollector inductively coupled plasma mass spectrometry: Reconsidering matrix interferences in bioapatites and biogenic carbonates. *Spectrochim. Acta B: At. Spectrosc.* **125**, 31–42 (2016).
63. Fasola, S., Muggeo, V. M. R. & Küchenhoff, H. A heuristic, iterative algorithm for change-point detection in abrupt change models. *Comput. Stat.* **33**, 997–1015 (2018).
64. Su, Y.-S. & Yajima, M. R2jags: Using R to Run 'JAGS'. R package version 0.6-1; 2020 (2021).
65. Plummer, M. JAGS: Just another Gibbs sampler (2023).
66. R Core Team. *R: A Language and Environment for Statistical Computing* (R Foundation for Statistical Computing, 2023).
67. Ayliffe, L. K. et al. Turnover of carbon isotopes in tail hair and breath CO_2 of horses fed an isotopically varied diet. *Oecologia* **139**, 11–22 (2004).
68. Cerling, T. E. et al. Determining biological tissue turnover using stable isotopes: the reaction progress variable. *Oecologia* **151**, 175–189 (2007).
69. Yang, D. Strontium isotope mapping of elephant enamel v. v0.9.3 (Zenodo, 2024).

Acknowledgements

The authors thank Nancy Carpenter and the Hogle Zoo for the agreement to loan Misha's dental material to the University of Utah. We thank elephant keeper Doug Thompkins and other zoo staff for their care for Misha during her time in Utah. We thank Scott Beld, Dan Davis, and Jared Singer for assistance with sample preparation, photomicroscopy, and isotope analyses. We thank Christopher Anderson for his help with the MC-ICP-MS analyses. KTU thanks Dan Fisher for his guidance and assistance in the preparation of the tusk material. We thank the associate editor Michele Repetto for handling this article. We thank Marius Robu, and two anonymous reviewers for their constructive comments that helped to improve this article. We thank Paul Koch for helpful suggestions that helped to improve an earlier version of this article. This project was supported by an AMNH Kalbfleisch Postdoctoral Research Fellowship awarded to DY, by a University of Utah Graduate Research Fellowship and Vetlesen Foundation (Columbia University) support awarded to KTU, and by the National Science Foundation grants EAR-2202880, DBI-1565128, and DBI-1759730 awarded to GJB, EAR-0819611 and BCS-0621542 awarded to TEC. This work was carried out under CITES permits US831854/9, 02US053837/9, and 07US159997/9.

Author contributions

D.Y. conceived the microsampling and modeling approach and developed the model code in discussion with the other authors. D.Y., K.P., K.T.U., D.P.F., and T.E.C. conducted the lab preparations and analyses. D.Y., K.P., K.T.U., and D.P.F. analyzed the data. GJB assisted with the structure and statistics of the model. K.T.U. and T.E.C. conceived the project associated with Misha's relocation. K.T.U., G.J.B., and T.E.C. and secured the funding.

D.Y. prepared a first draft of the manuscript, and all authors contributed critically to successive drafts and gave final approval for publication.

Competing interests

The authors declare no competing interests.

Additional information

Supplementary information The online version contains supplementary material available at <https://doi.org/10.1038/s42003-025-07686-9>.

Correspondence and requests for materials should be addressed to Deming Yang.

Peer review information *Communications Biology* thanks Marius Robu and the other, anonymous, reviewer(s) for their contribution to the peer review of this work. Primary Handling Editor: Michele Repetto. A peer review file is available.

Reprints and permissions information is available at <http://www.nature.com/reprints>

Publisher's note Springer Nature remains neutral with regard to jurisdictional claims in published maps and institutional affiliations.

Open Access This article is licensed under a Creative Commons Attribution-NonCommercial-NoDerivatives 4.0 International License, which permits any non-commercial use, sharing, distribution and reproduction in any medium or format, as long as you give appropriate credit to the original author(s) and the source, provide a link to the Creative Commons licence, and indicate if you modified the licensed material. You do not have permission under this licence to share adapted material derived from this article or parts of it. The images or other third party material in this article are included in the article's Creative Commons licence, unless indicated otherwise in a credit line to the material. If material is not included in the article's Creative Commons licence and your intended use is not permitted by statutory regulation or exceeds the permitted use, you will need to obtain permission directly from the copyright holder. To view a copy of this licence, visit <http://creativecommons.org/licenses/by-nc-nd/4.0/>.

© The Author(s) 2025